Proceedings of the ASME 2018 International Design Engineering Technical Conferences & Computers and Information in Engineering Conference
IDETC/CIE 2018
August 26-August 29, 2018, Quebec City, Quebec, Canada

DETC2018-85826

THERMAL PRESTRESS IN COMPOSITE COMPLIANT SHELL MECHANISMS

Jonathan P. Stacey*
Bristol Composites Institute (ACCIS)
Department of Aerospace Engineering
University of Bristol
Bristol, BS8 1TR, United Kingdom
Email: jonathan.stacey@bristol.ac.uk

Matthew P. O'Donnell
Mark Schenk
Bristol Composites Institute (ACCIS)
Department of Aerospace Engineering
University of Bristol
Bristol, BS8 1TR, United Kingdom

ABSTRACT

Due to the anisotropic nature of fibre-reinforced laminates, thermally-induced internal stresses can remain in the material after manufacture. Mismatches between coefficients of thermal expansion are especially prominent in thin shells with fewer plies or large angle variations. Such stresses cause out-of-plane warping and are therefore often deliberately avoided. Utilising their effects on structural behaviour however, can enable stiffness-tailored composite compliant mechanisms. Work detailed in this paper aims to exploit thermal prestress to reduce the torsional stiffness of cross-ply tape laminate springs.

An extension of an analytical tape spring model with composite thermal analysis is presented, which shows that thermal effects cause significant changes to the energy landscapes of thin composite shells. Tape springs that would otherwise be monostable structures become bistable and exhibit greater ranges of low-energy twisting when thermally-induced prestress is present. Predicted shell geometries are compared with finite element models and manufactured samples, showing good agreement between all approaches. The limited feasibility of zero torsional stiffness composite tape springs is discussed, as well as wider challenges involved in manufacturing prestressed composite compliant mechanisms such as fibre misalignment and moisture ingress.

*Address all correspondence to this author.

INTRODUCTION

Compliant shell mechanisms are thin shell structures that are capable of large deflection and small strain elastic deformations. In addition to enabling tailorable force and displacement responses, a significant advantage of such mechanisms is the lack of need for mechanical joints, in turn removing friction and reducing maintenance requirements. While the optimised design of compliant mechanisms has been studied for isotropic materials [1, 2], composite materials offer unique benefits to the mechanism designer. These benefits include high specific properties, anisotropic deformation behaviour, ease of manufacturing complex geometries, and new ways of tailoring the residual stress state of the mechanism. This study aims to investigate the effects of thermal prestress, arising from mismatches in thermal expansion coefficients [3], on the behaviour of composite tape springs. This is achieved using extensions of existing analytical approaches that are compared to experimental results and finite element (FE) simulations.

Tape springs are a class of structures that have been widely investigated as compliant mechanisms [4, 5]. Analytical models, used to gain insight into their behaviour, often contain a careful balance of geometric and prestress effects that allows desirable behaviour, such as bi-stability [6] or zero-stiffness [5, 7, 8]. In classical mechanisms multiple members would be required to enable such behaviour [9–11]. In particular, we utilise the model of Guest and Pellegrino [4] which assumes the behaviour can be described by a tape spring that is assumed to be kinematically

constrained to the surface of an underlying cylinder. We extend this approach by utilising anisotropic composite materials, enabling the exploitation of their desirable stiffness characteristics and thermal behaviour. The feasibility of zero torsional stiffness tape springs is discussed. Such compliant mechanisms have potential for applications in medical exoskeletons [12], deployable spacecraft structures [13], and morphing aerostructures [14].

As well as geometry and material considerations, the design space for general compliant mechanisms includes residual stress states. Residual thermal prestress due to composite manufacturing has been subject of extensive research efforts. While ongoing research aims to describe localised thermal effects and warping in detail [15], classical laminate analysis (CLA), such as described by Nettles [16], provides a sufficiently accurate model of thin composite behaviour, and is used in this paper. Other effects such as viscoelastic relaxation can also affect prestress [17–19], but are beyond the scope of this work. Laminates with non-symmetrical layups often exhibit warp due to the mismatch between thermal expansion coefficients between plies, and as such are often deliberately avoided [20]. However, these thermal effects can be used to provide prestress [21], which help obtain desirable behaviour in tape springs and other thin shell structures [14, 22, 23]. We modify the model of Guest and Pellegrino [4] to include these thermal effects, showing that the low-energy twisting region greatly increases, and we demonstrate that our extended tape spring model correlates well with FE models and manufactured samples.

This paper aims to evaluate the potential of using thermal prestress in the design of stiffness-tailored compliant shell mechanisms. Specifically, we focus on reducing torsional stiffness within composite tape springs and evaluating the feasibility of zero torsional stiffness prestressed structures. The paper is structured as follows. First, the analytical approach is detailed, including rationale behind material selection, derivation of the strain energy equation and comparisons of energy landscapes. Next, two sections detail validation work: FE modelling and the manufacture of sample tape springs. The results of each approach are discussed and compared before final conclusions are presented.

ANALYTICAL MODEL

Material and Layup Selection

To ascertain the upper limits of potential of prestressed composite compliant mechanisms, a layup and material configuration was selected which would exhibit the maximum thermally-induced bending moments per unit thickness. A cross ply laminate configuration – where the fibres in the bottom half of the laminate lie perpendicular to those in the upper half – was found to be most suitable. This provides the greatest overall mismatch of thermal expansion coefficients through the laminate thickness. Wider ranges of composite laminate layups are beyond the scope of the current work.

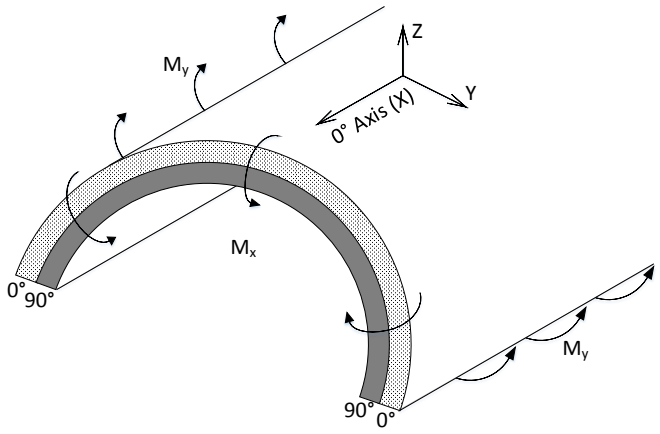

FIGURE 1. CROSS-SECTIONAL REPRESENTATION OF A CROSS-PLY TAPE SPRING SHOWING DIRECTIONS OF BENDING MOMENTS RESULTING FROM POST-CURE COOLING

TABLE 1. MATERIAL DATA IM7-8552

$E_{11} = 161$ GPa	$\alpha_{11} = -0.1 \cdot 10^{-6}$ K^{-1}
$E_{22} = 11.38$ GPa	$\alpha_{22} = 31 \cdot 10^{-6}$ K^{-1}
$G_{12} = 5.17$ GPa	$t = 0.131$ mm
$\nu_{12} = 0.32$	$\rho = 1.57 \cdot 10^{3}$ kg/m^{3}

Tape springs were chosen as a representative compliant mechanism due to their ease of manufacture and well-understood mechanical behaviour. By placing fibres at 90° to the longitudinal axis on the inner surface of the tape spring (*i.e.* $[90_N/0_N]$, where N is a positive integer representing the number of plies) the bending moments produced upon cooling would be similar to those produced by mechanically prestressed isotropic tape springs (such as those presented by Guest *et al.* [5]). The thermal strains in such cross-ply laminates produce a 'coiling-up' moment, M_x, in the longitudinal direction, and an 'opening-out' moment, M_y, in the hoop direction (see Figure 1). Existing tape spring models were used as a starting point for analytical investigations.

Carbon fibre composites were chosen due to their high specific stiffness and low creep characteristics relative to glass and aramid fibre reinforcements, as well as its suitable thermal expansion properties. Hexcel IM7-8552 was used as a benchmark composite material due to its general availability and well-characterised properties [24]; see Table 1.

Elastic Strain Energy

In this work, the effect of thermal prestress on the energy landscape of anisotropic composite tape spring is considered. Following Guest and Pellegrino [4], the strain energy, U, stored by the tape spring per unit area, is described by

$$U = \frac{1}{2}(\Delta\boldsymbol{\kappa}^T \boldsymbol{D}^* \Delta\boldsymbol{\kappa}) \tag{1}$$

where $\boldsymbol{D}^*$ is the reduced bending stiffness matrix

$$\boldsymbol{D}^* = \boldsymbol{D} - \boldsymbol{B}^T \boldsymbol{A}^{-1} \boldsymbol{B} \tag{2}$$

and $\boldsymbol{A}$, $\boldsymbol{B}$ and $\boldsymbol{D}$ are the in-plane, coupling and bending stiffness matrices of CLA [16]. The $\boldsymbol{D}^*$ matrix accounts for the contribution of non-zero $\boldsymbol{B}$ matrices to the strain energy [4].

The strain energy equation can be nondimensionalised as

$$\hat{U} = U\frac{R^2}{D_{11}^*} \tag{3}$$

using the manufacture tooling radius, R, and the reduced bending stiffness term, D_{11}^* [4].

In the Guest and Pellegrino model, an inextensional tape spring shell element (with existing curvature in the y-direction) is rotated around an underlying cylinder to investigate the curvature changes, $\Delta\boldsymbol{\kappa}$, that occur during twist. The modification made in this work is that change in curvature

$$\Delta\boldsymbol{\kappa} = \boldsymbol{\kappa}_{cylinder} - \boldsymbol{\kappa}_{warped} \tag{4}$$

is measured with respect to a thermally-warped element with curvatures $\boldsymbol{\kappa}_{warped}$, rather than an element with only curvature κ_y. Thus, the strain energy calculated will be that required to conform the warped element to the underlying cylinder ($\boldsymbol{\kappa}_{cylinder}$).

The curvature of the tape spring on the underlying cylinder is based on a Mohr's circle of curvature

$$\boldsymbol{\kappa}_{cylinder} = \frac{C}{2}\begin{bmatrix} 1-\cos(2\theta) \\ 1+\cos(2\theta) \\ 2\sin(2\theta) \end{bmatrix} \tag{5}$$

where θ refers to the twist angle, and C the curvature of an underlying cylinder [5]. For this model to remain valid, the post-cure tape spring geometry must approximately conform to an underlying cylinder.

The curvature of the thermally warped tape spring (*i.e.* the origin state) is defined as

$$\boldsymbol{\kappa}_{warped} = \begin{bmatrix} 0 \\ 1/R \\ 0 \end{bmatrix} + \Delta\boldsymbol{\kappa}^{th} \tag{6}$$

where the thermal curvature changes during cooling from manufacture, $\Delta\boldsymbol{\kappa}^{th}$ are added to the manufacture tooling radius. The changes in curvature of an anisotropic plate due to thermally-induced bending moments ($\boldsymbol{M}^{th}$) and in-plane forces ($\boldsymbol{N}^{th}$) [3] can be evaluated as

$$\Delta\boldsymbol{\kappa}^{th} = \begin{bmatrix} \Delta\kappa_x^{th} \\ \Delta\kappa_y^{th} \\ \Delta\kappa_{xy}^{th} \end{bmatrix} = -\Delta T(\boldsymbol{D}^*)^{-1}(\boldsymbol{M}^{th} - \boldsymbol{B}\boldsymbol{A}^{-1}\boldsymbol{N}^{th}) \tag{7}$$

where a negative sign is added to align the sign conventions in CLA with the underlying cylinder model.

The thermal moments $\boldsymbol{M}^{th}$ and in-plane forces $\boldsymbol{N}^{th}$ per degree Celsius are given as

$$\boldsymbol{M}^{th} = \begin{bmatrix} M_x^{th} \\ M_y^{th} \\ M_{xy}^{th} \end{bmatrix} = \frac{H^2}{8}\begin{bmatrix} W_2^{th}\xi_5 \\ -W_2^{th}\xi_5 \\ W_2^{th}\xi_7 \end{bmatrix} \tag{8}$$

and

$$\boldsymbol{N}^{th} = \begin{bmatrix} N_x^{th} \\ N_y^{th} \\ N_{xy}^{th} \end{bmatrix} = \frac{H}{2}\begin{bmatrix} W_1^{th} + W_2^{th}\xi_1 \\ W_1^{th} - W_2^{th}\xi_1 \\ W_2^{th}\xi_3 \end{bmatrix} \tag{9}$$

with lamination parameters ξ

$$\xi_1 = \frac{(A_{11} - A_{22})}{2W_2H}$$
$$\xi_3 = \frac{(A_{16} + A_{26})}{W_2H}$$
$$\xi_5 = \frac{2(B_{11} - B_{22})}{W_2H^2}$$
$$\xi_7 = \frac{4(B_{16} + B_{26})}{W_2H^2}$$

and material invariants W and W^{th}

$$W_2 = \frac{1}{2}(Q_{11} - Q_{22})$$
$$W_1^{th} = \alpha_{11}Q_{11} + (\alpha_{11} + \alpha_{22})Q_{12} + \alpha_{22}Q_{22}$$
$$W_2^{th} = \alpha_{11}Q_{11} + (\alpha_{22} - \alpha_{11})Q_{12} + \alpha_{22}Q_{22}$$

where H is the laminate thickness, α refers to coefficients of thermal expansion, and Q is the reduced ply stiffness (standard CLA notation) [3]. Lamination parameters allow any laminate to be described by twelve terms and the total thickness [25]. This approach is particularly valuable for complex combinations of fibre angles, and for optimisation of laminate lay-ups.

Stability Analysis

Equilibrium configurations of the anisotropic tape spring in the twisting domain are found by setting $\partial U/\partial\theta$ equal to zero. This first partial differential is expressed as

$$\frac{\partial U}{\partial\theta} = \frac{C}{4R}(\lambda_1\sin(2\theta)+\lambda_2\cos(2\theta)... + \lambda_3\sin(4\theta)+\lambda_4\cos(4\theta)) = 0 \tag{10}$$

where

$$\begin{aligned}
\lambda_1 &= 4(D^*_{22}-D^*_{12})+2CR(D^*_{11}-D^*_{22})...\\
&\quad +4R(\Delta\kappa^{th}_x(D^*_{12}-D^*_{11})...\\
&\quad\quad +\Delta\kappa^{th}_y(D^*_{22}-D^*_{12})...\\
&\quad\quad +\Delta\kappa^{th}_{xy}(D^*_{26}-D^*_{16}))\\
\lambda_2 &= 4CR(D^*_{16}+D^*_{26})...\\
&\quad -8(\Delta\kappa^{th}_x D^*_{16}+(\Delta\kappa^{th}_y+1)D^*_{26}+\Delta\kappa^{th}_{xy}D^*_{66})\\
\lambda_3 &= CR(4D^*_{66}+2D^*_{12}-D^*_{22}-D^*_{11})\\
\lambda_4 &= 4CR(D^*_{26}-D^*_{16})
\end{aligned}$$

A zero-stiffness structure will exhibit no change in internal strain energy throughout the designed mode of deformation, and will thus be in constant equilibrium. Guest *et al.* [5] describe a zero torsional stiffness tape spring, with isotropic material properties and mechanically introduced prestress.

For composites, a general solution of Equation 10 is non-trivial even when simplified for cross-ply laminates, where $D^*_{16} = D^*_{26} = 0$. Furthermore the differential with respect to underlying cylinder curvature, $\partial U/\partial C$, would also have to equal zero, increasing the complexity of the problem. Mapping the boundaries of potential zero stiffness regions remains an ongoing area of investigation.

The second differential provides insight into stability of the equilibria in the tape spring energy landscape:

$$\frac{\partial^2 U}{\partial\theta^2} = \frac{C}{2R}(\lambda_1\cos(2\theta)-\lambda_2\sin(2\theta)... + 2\lambda_3\cos(4\theta)-2\lambda_4\sin(4\theta)) = 0 \tag{11}$$

Equation 11 shows that for the zero twist (*i.e.* as-manufactured, $\theta = 0°$) condition to be stable, $\lambda_1+2\lambda_3 \geq 0$, and for a coiled configuration (*i.e.* $\theta = 90°$) to be stable, $\lambda_2+2\lambda_4 \geq 0$. These conditions will be explored further in future work.

Energy Landscape Comparisons

Figure 2 shows polar plots of nondimensional strain energy as a function of tape spring twist, 2θ, and underlying cylinder curvature, C. The tape spring is a $[90_2/0_2]$ IM7-8552 composite laminate shell with a manufactured radius of 38 mm. A $\Delta T = -155$°C models the cool down from a typical 180°C cure to room temperature. The post-warp shape was found to remain nominally cylindrical, as per the model assumptions.

Figure 2A shows the energy landscape for a cross-ply tape spring with no thermal prestress: it is monostable with a low energy ($\hat{U}$<0.1) twisting region of approximately ±20°. The low energy twist behaviour is due to the open cross-section of the tape spring. Figure 2B shows the effect of a thermally-induced prestress: the structure becomes bistable, with an unstable zero twist configuration. The low-energy twisting region increases to approximately ±45°, illustrating the potential for using thermal prestress to reduce the torsional stiffness of thin shell composite structures. Figure 2C shows the effect of fibre misalignment on the thermally prestressed shells. A misalignment of 2° in the inner two plies causes a slight rotation of the energy landscape, resulting in a pseudo-bistable structure where one twisted mode is favoured over the other. While the energy landscape is different, the location of equilibria and the range of the low energy twisting region are similar to the non-misaligned tape spring.

FINITE ELEMENT MODEL

Model Setup

As a first method to verify the energy landscapes, FE models were made for the tape springs. These models were built in Abaqus/Standard, and were meshed using S4R shell elements of 5×5 mm target size. A fully-fixed boundary condition is applied to the central node.

After defining the composite layup, the post-cure cooling process is modelled by applying two predefined temperature fields to the tape spring: (i) the expected cure temperature (180°C), (ii) assumed room temperature (25°C), to give $\Delta T = -155$°C. An example of the resulting deformed shape can be seen in Figure 3A.

Twisted Configurations

The warped shape shown in Figure 3A exists in a zero-twist configuration. The curling effects seen at the ends are due to residual moments from the thermal prestressing. A prestressed $[90_N/0_N]$ cross-ply tape spring in this configuration is predicted to be unstable (see Figure 2B), but the stable twisted configurations will not be identified with FE without breaking the model

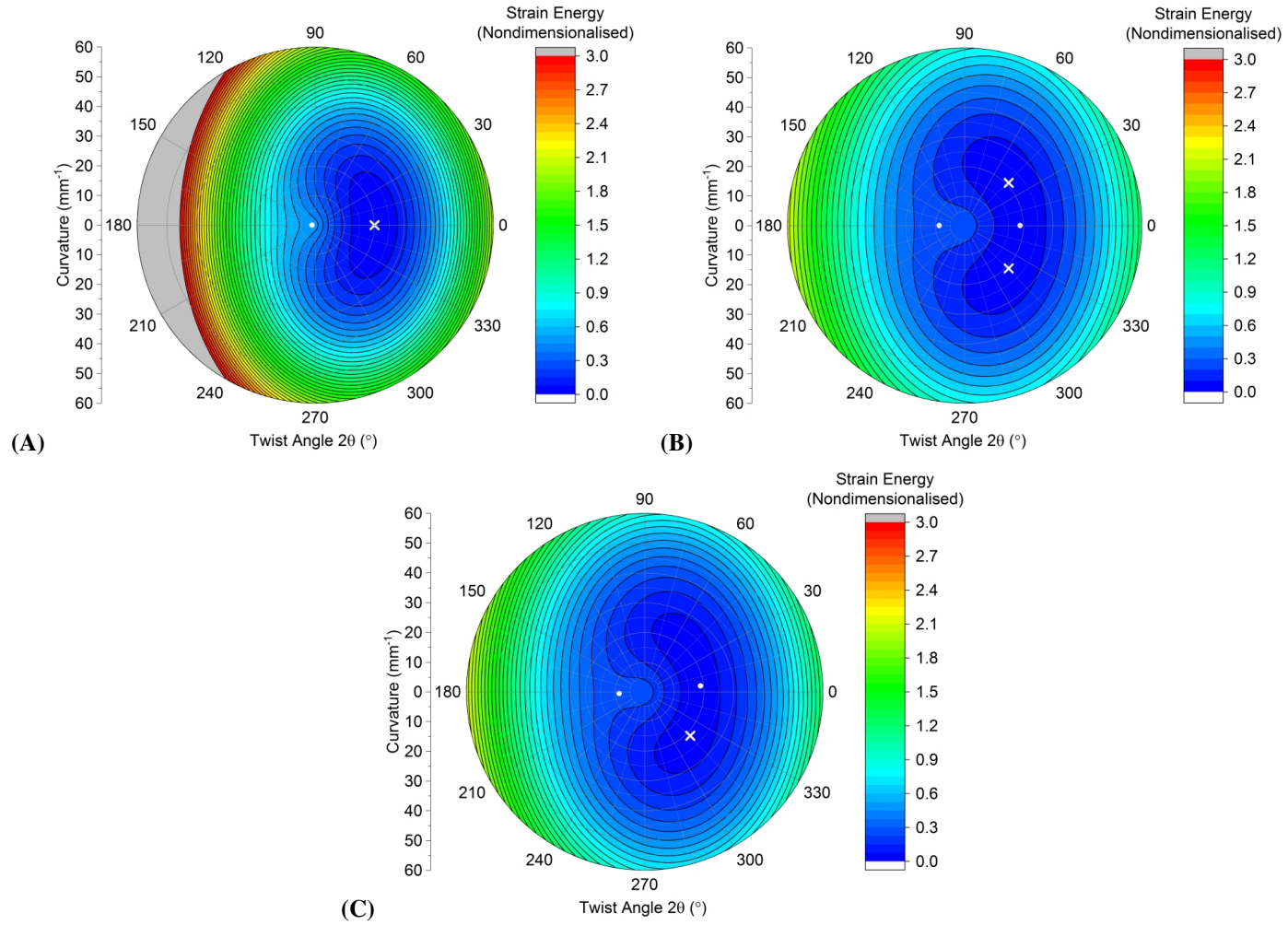

FIGURE 2. POLAR PLOTS OF NONDIMENSIONAL ENERGY $\hat{U}$ AS A FUNCTION OF TAPE SPRING TWIST, 2θ, ON THE ANGULAR AXIS, AND CYLINDER CURVATURE, C, ON THE RADIAL AXIS. CONTOURS ARE PLOTTED FOR $\hat{U}$ VALUES BETWEEN 0.0 TO 3.0 INCLUSIVE WITH INTERVALS OF 0.1; (A) SHOWS THE LANDSCAPE FOR A $[90_2/0_2]$ TAPE SPRING WITH MANUFACTURED RADIUS $R = 38$ MM WITH NO THERMAL PRESTRESS, (B) SHOWS THE LANDSCAPE FOR A THERMALLY PRESTRESSED TAPE SPRING, AND (C) SHOWS THE SAME LANDSCAPE AS SUBFIGURE (B), BUT FOR A MISALIGNED LAYUP OF $[88_2/0_2]$; POINTS LABELLED WITH A CROSS INDICATE THE STABLE STATE(S), AND DOTS INDICATE UNSTABLE EQUILIBRIA.

symmetry. To achieve this, a small fibre misalignment was applied to each 90° ply in the laminate until a twisted structure was produced (-2° for the 38 mm radius springs; -5° for the 50 mm radius spring). Energy landscapes of tape springs with fibre misalignment (see example Figure 2C) were considered sufficiently similar to those without, that direct comparisons could be drawn between the 'misaligned' FE models and the other investigative approaches. An example twisted structure prediction can be seen in Figure 3B.

PROTOTYPE MANUFACTURE

Design Curvature

By considering only thermal affects, a design radius can be determined that will give a zero final (*i.e.* post cure warping) curvature for a given set of material properties. The expected $\Delta\kappa_y^{th}$ for a tape spring manufactured with initial κ_y can be evaluated using Equation 7. By choosing the initial κ_y (*i.e.* the curvature of the manufacturing tooling) that is equal and opposite to the predicted $\Delta\kappa_y^{th}$, the curvatures can be cancelled. For a [90/0] cross-ply laminate made from IM7-8552, this equates to a tooling radius of approximately 55 mm, and represents the limit at

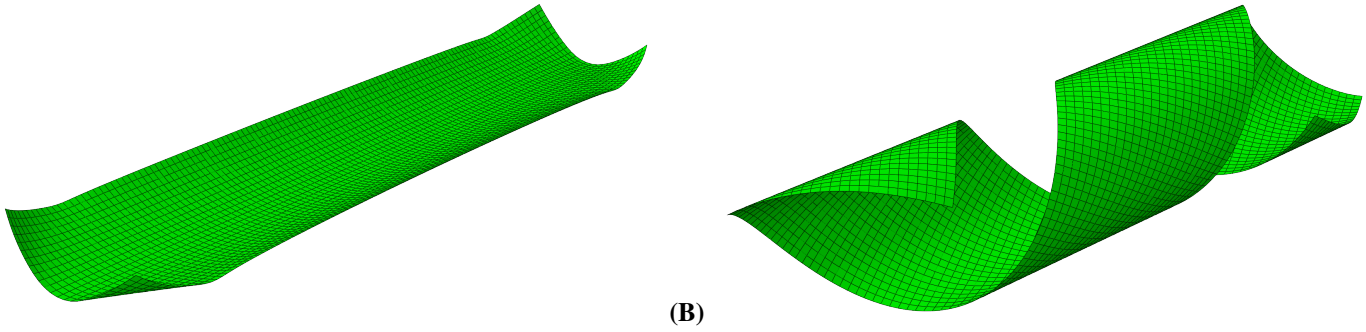

(A) **(B)**

FIGURE 3. FE PREDICTIONS OF (A) THE UNSTABLE UNTWISTED POST-WARP SHAPE, AND (B) THE STABLE TWISTED SHAPE FOR A [90/0] LAYUP WITH TOOL RADIUS $R = 38$ MM.

which the warped tape spring is cylindrical.

At this limit, the analytical model is likely to be inaccurate due to the assumption of an underlying cylinder. Steel tooling of radius 38 mm and 50 mm was selected for ply layup to ensure that manufactured tape springs were within this limit, where the model assumptions would still be valid. A code *RXXTN* describes each sample, where *XX* refers to the manufactured tool radius (mm) and *N* refers to the layup $[90_N/0_N]$.

Manufacturing Process

A manual layup and vacuum-bagging process was used before curing the samples in an autoclave. Plies of pre-impregnated (prepreg) carbon fibre (IM7-8552) were laid-down to create rectangular plates with a $[90_N/0_N]$ layup. The prepreg plates were then placed on metal tubes to provide the design curvature, with the 0° fibre direction aligning with the tube cylindrical axis. The inner 90° plies were separated from the tool surface by a layer of release film. Due to the difficulty in laying 90° fibres around a curved surface, a heat gun was used periodically to increase the prepreg tackiness and encourage adhesion to the tool surface. Once the layup was complete, an envelope bag was constructed around the tube, and a vacuum was applied to consolidate the plies on the tool. The samples were then cured at 7 bar pressure and 180°C in the autoclave.

Profile Measurement

Once cured, the geometric information of the plies was recorded using a FARO Edge ScanArm® optical measurement device and associated CAM2 Measure 10.7 software. This device consists of a laser scanning probe mounted upon a moveable arm, and generates a 'cloud' of *XYZ* data points of complex geometries.

The cured tape springs were allowed to cool down to ambient temperature before being released from their vacuum bags (to minimise moisture uptake from the atmosphere that could affect

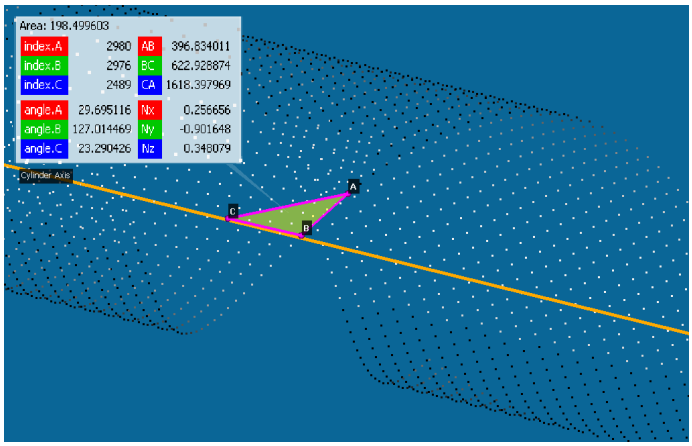

FIGURE 4. TWIST ANGLE MEASUREMENT USING POINT CLOUD AND UNDERLYING CYLINDER AXIS

twisted geometry). Once cooled, the samples were de-bagged and mass readings were immediately taken to establish a nominally zero-moisture benchmark, and geometric scans were conducted within 24 hours.

The first parameter used for validation was the helical twist angle, defined as the angle of orientation of the twisted shell with respect to the length-wise axis of an underlying cylinder. This angle was measured by analysing the sample point clouds using an open-source software called CloudCompare [26]; see Figure 4. The second parameter, underlying curvature, is directly measured from a fitted cylinder. FE and experimental results for the same tape spring can be seen in Figure 3B and Figure 5 respectively. The difference in twist direction is due to the arbitrary choice of fibre angle misalignment direction in the FE model.

Point clouds were also generated from the deformed nodal positions of the FE models, with helical twist angle and underlying curvature measured in the same manner.

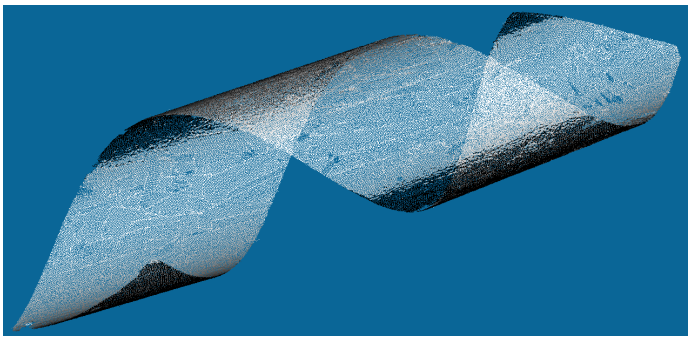

FIGURE 5. LASER SCAN POINT CLOUD FOR SAMPLE R38T1

After FE-predicted geometries and manufactured sample geometries had been recorded, comparisons could be made between all three approaches to verify the analytical energy landscapes.

RESULTS & DISCUSSION

Comparisons between the calculated stable twisted configurations, and the results for different twist angles and helix cylinder radii are given in Table 2; the corresponding energy plots for each sample are shown in Figure 6. Experimental results for R50T1 were from visual inspection and not point cloud measurement due to the spring being almost completely coiled post-cure and thus impractical for laser scanning.

Table 2 shows good agreement between the analytical and FE models for both twist angles (range within 2°) and helix radii (range within 3mm). There is also good agreement with the experimental results. The discrepancies could be attributed to manufacturing sensitivity of thin-shell composites, a higher ΔT observed in the manufactured samples, as well moisture ingress between manufacture and measurement.

Interestingly, after one week the twist angle of R38T2 reduced by around 65%. It is hypothesised this is due to viscoelastic relaxation and moisture ingress, and its 'relaxation' effect on thermal stresses [27, 28]. While controlling temperature during manufacture is possible, controlling the usage temperature and ambient moisture – and hence mechanical behaviour – of thermally prestressed compliant shells is much more challenging. A compliant mechanism relying purely on thermal prestress may behave differently depending on the weather or time of year, thus some degree of active thermal control may be necessary depending on the application and required mechanical responses.

Figure 7B shows R50T1 after a week-long exposure to the ambient environment: the reduction in twist angle (and extension in length) can be clearly seen compared to Figure 7A. The relaxation is a short-term effect: bi-stable samples tended to favour one twist direction within hours (in contradiction to energy landscape predictions in Figure 6), potentially accentuating any fibre misalignment effects from manufacturing. Storing samples in a desiccator will mitigate against moisture effects. Quantifying the degree of recovery from moisture effects, as well as the impact of moisture on design spaces remains the subject of ongoing investigation.

Finally, it was possible to induce non-cylindrical stable shapes with R50T1 by manually twisting and buckling the sample. One such stable configuration can be seen in Figure 7C, and highlights the limitations of assuming that the underlying deformed shell structure is cylindrical. If a general approach for designing composite compliant shells is to be realised, then a less geometrically-restrictive model is required.

CONCLUSIONS

In conclusion, making use of the residual stresses in a cross-ply laminate has been shown to increase the range of twist angles that can be achieved at very low ($\hat{U}<0.1$) levels of internal strain energy. An extension of existing composite tape spring models [4] incorporating thermal effects has been presented, as well as finite element simulations and experimental samples of tape springs of different thickness and manufactured radius. All approaches were shown to have good agreement in predicting the tape spring twisted states. Very good agreement for helical twist angle and radius was shown between theoretical and FE predictions, with experimental results indicating that these structures are sensitive to manufacturing variations. Moreover, some unusual buckled shapes seen in sample tape springs indicate that the analytical and FE models are not fully capable of capturing every stable tape spring configuration.

The feasibility of a composite tape spring with zero torsional stiffness has also been discussed. A zero stiffness solution has been shown to be non-trivial, even for cross-ply laminates where D^*_{16} and D^*_{26} effects are removed. Further work is required to more generally quantify the limits of stiffness reduction achievable using thermal prestress.

Several other design-influencing factors have been identified, including temperature control, moisture-driven behaviour changes and experimental measurement methods. These factors must be addressed for a practical thermally prestressed composite shell to be realised, and each present interesting avenues for further study. Future areas of work include refinement of measurement methods, measuring shape recovery by drying samples, and investigations into any long term viscoelastic relaxation.

ACKNOWLEDGMENT

The work detailed in this paper was funded by the Engineering and Physical Sciences Research Council (EPSRC) as part of the Centre for Doctoral Training in Advanced Composites for Innovation and Science (grant number EP/L016028/1). All data

TABLE 2. OVERALL TWIST ANGLES AND UNDERLYING CYLINDER RADII

	Manufacture			Helix Radius (mm)			Twist Angle (°)		
Sample	Layup	Radius (mm)	ΔT (°C)	Theory	FE	Experiment	Theory	FE	Experiment
R38T2	$[90_2/0_2]$	38	-162.7	48.1	50.6	50.9	22	21.8	16.9
R38T2 (+1 wk)	$[90_2/0_2]$	38	-162.7	48.1	-	47.4	22	-	6.0
R38T1	$[90/0]$	38	-163.9	48.1	47.3	55.5	55	53.0	47.8
R50T1	$[90/0]$	50	-164.6	63.3	-	80	87	-	90

required to reproduce the results shown is contained within this paper.

Thanks go to Prof. Just Herder, Werner van de Sande and Giuseppe Radaelli (TU Delft) for their support and helpful discussions about compliant mechanisms, as well as Boudewijn Wisse (Laevo BV) for sharing his insights into compliant mechanism technology in exoskeletons.

REFERENCES

[1] Radaelli, G., and Herder, J., 2014. "Isogeometric Shape Optimization for Compliant Mechanisms With Prescribed Load Paths". In Proc. ASME 2014 Int. Des. Eng. Tech. Conf. Comput. Inf. Eng. Conf.

[2] Radaelli, G., and Herder, J., 2016. "A monolithic compliant large-range gravity balancer". *Mech. Mach. Theory,* ***102***, aug, pp. 55–67.

[3] Weaver, P., O'Donnell, M., and York, C., 2010. "Approximations for Warp-Free Laminate Configurations". In 51st AIAA/ASME/ASCE/AHS/ASC Struct. Struct. Dyn. Mater. Conf. 18th AIAA/ASME/AHS Adapt. Struct. Conf.

[4] Guest, S., and Pellegrino, S., 2006. "Analytical models for bistable cylindrical shells". *Proc. R. Soc. A Math. Phys. Eng. Sci.,* ***462***(2067), mar, pp. 839–854.

[5] Guest, S., Kebadze, E., and Pellegrino, S., 2011. "A zero-stiffness elastic shell structure". *J. Mech. Mater. Struct.,* ***6***(1-4), jun, pp. 203–212.

[6] Seffen, K., and Guest, S., 2011. "Prestressed Morphing Bistable and Neutrally Stable Shells". *J. Appl. Mech.,* ***78***(1), p. 011002.

[7] Murphey, T., and Pellegrino, S., 2004. "A Novel Actuated Composite Tape-Spring for Deployable Structures". In 45th AIAA/ASME/ASCE/AHS/ASC Struct. Struct. Dyn. Mater. Conf.

[8] Schultz, M., Hulse, M., Keller, P., and Turse, D., 2008. "Neutrally stable behavior in fiber-reinforced composite tape springs". *Compos. Part A Appl. Sci. Manuf.,* ***39***(6), pp. 1012–1017.

[9] Morsch, F., and Herder, J., 2010. "Design of a Generic Zero Stiffness Compliant Joint". In Proc. ASME 2010 Int. Des. Eng. Tech. Conf. Comput. Inf. Eng. Conf.

[10] Herder, J., Barents, R., Schenk, M., van Dorsser, W., and Wisse, B., 2011. "Spring-to-Spring Balancing as Energy-Free Adjustment Method in Gravity Equilibrators". *J. Mech. Des.,* ***133***(June 2011), p. 061010.

[11] Schenk, M., and Guest, S., 2014. "On zero stiffness". *Proc. Inst. Mech. Eng. Part C J. Mech. Eng. Sci.,* ***228***(10), pp. 1701–1714.

[12] Nijssen, J., 2016. "A Type Synthesis Approach to Compliant Shell Mechanisms". Application, Delft University of Technology.

[13] Murphey, T., Francis, W., Davis, B., and Mejia-Ariza, J., 2015. "High Strain Composites". In 2nd AIAA Spacecr. Struct. Conf.

[14] Lachenal, X., Daynes, S., and Weaver, P., 2013. "A zero torsional stiffness twist morphing blade as a wind turbine load alleviation device". *Smart Mater. Struct.,* ***22***(6), p. 065016.

[15] Cantera, M., Romera, J., Adarraga, I., and Mujika, F., 2014. "Modelling of [0/90] laminates subject to thermal effects considering mechanical curvature and through-the-thickness strain". *Compos. Struct.,* ***110***(1), apr, pp. 77–87.

[16] Nettles, A., 1994. Basic mechanics of laminated composite plates. Tech. Rep. October 1994, NASA Marshall Space-flight Centre.

[17] Fancey, K., and Pang, J., 2009. "The flexural stiffness characteristics of viscoelastically prestressed polymeric matrix composites". *Compos. Part A Appl. Sci. Manuf.,* ***40***(6-7), pp. 784–790.

[18] Brinkmeyer, A., Pellegrino, S., and Weaver, P., 2015. "Effects of Long-Term Stowage on the Deployment of Bistable Tape Springs". *J. Appl. Mech.,* ***83***(1), nov, p. 011008.

[19] Fancey, K., and Fazal, A., 2016. "Prestressed polymeric matrix composites: Longevity aspects". *Polym. Compos.,* ***37***(7), jul, pp. 2092–2097.

[20] Mansfield, E., 1989. *The Bending & Stretching of Plates*, 2nd ed. Cambridge University Press.

[21] Daynes, S., and Weaver, P., 2013. "Stiffness tailoring us-

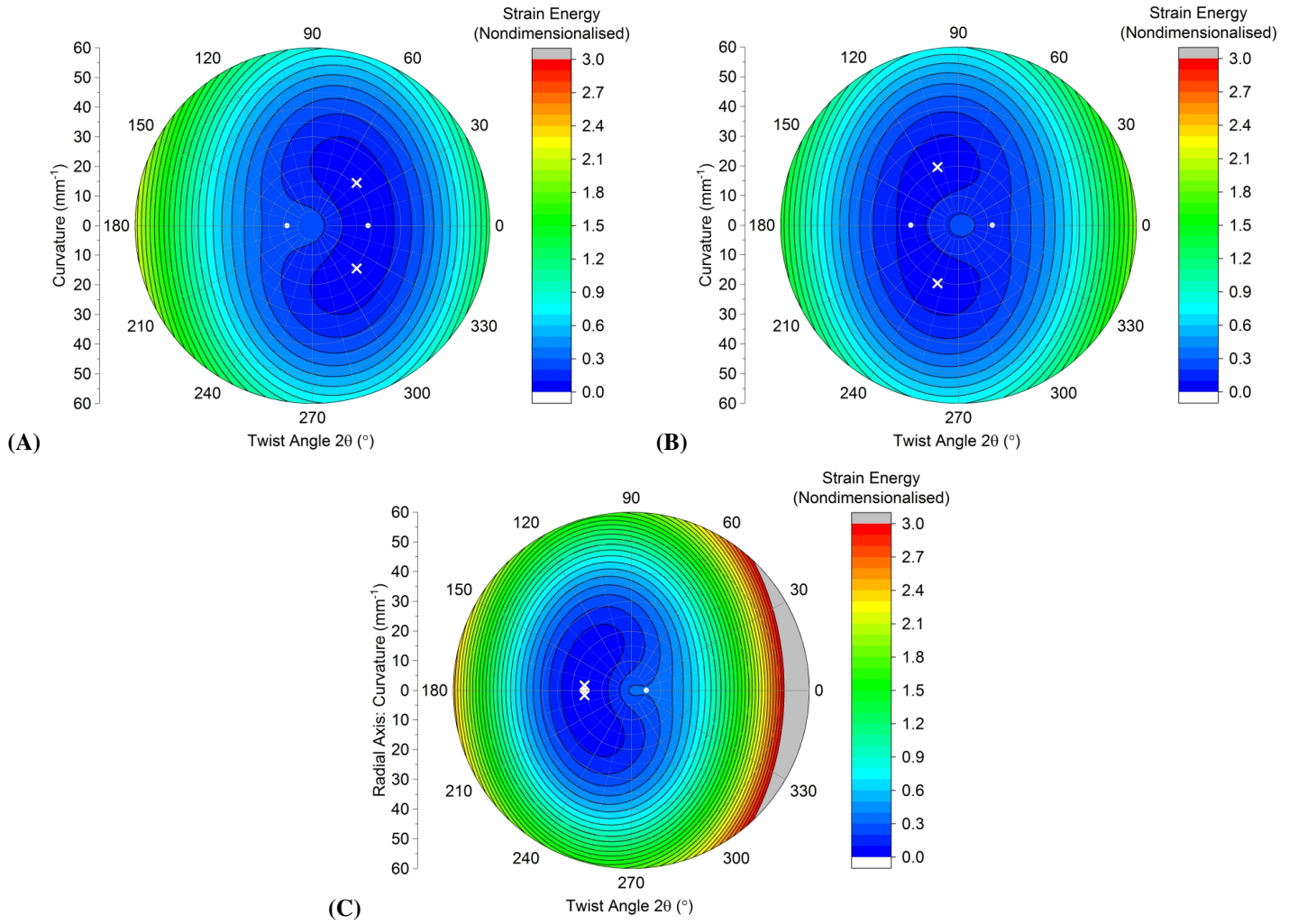

FIGURE 6. POLAR PLOTS OF NONDIMENSIONAL ENERGY $\hat{U}$ AS A FUNCTION OF TAPE SPRING TWIST, 2θ, ON THE ANGULAR AXIS, AND CYLINDER CURVATURE, C, ON THE RADIAL AXIS. CONTOURS ARE PLOTTED FOR $\hat{U}$ VALUES BETWEEN 0.0 TO 3.0 INCLUSIVE WITH INTERVALS OF 0.1; SUBFIGURES SHOW (A) R38T2, (B) R38T1, AND (C) R50T1. ALL PREDICT UNSTABLE ON-TOOL CONFIGURATIONS, WITH (A) AND (B) BEING CLEAR BISTABLE TWISTED STRUCTURES, AND (C) ALMOST A MONOSTABLE COILED STRUCTURE. POINTS INDICATED BY A CROSS REPRESENT STABLE STATE(S) AND DOTS INDICATE UNSTABLE EQUILIBRIA.

ing prestress in adaptive composite structures". *Compos. Struct.,* ***106***, pp. 282–287.

[22] Pirrera, A., Lachenal, X., Daynes, S., Weaver, P., and Chenchiah, I., 2013. "Multi-stable cylindrical lattices". *J. Mech. Phys. Solids,* ***61***(11), pp. 2087–2107.

[23] Lachenal, X., Weaver, P., and Daynes, S., 2012. "Multi-stable composite twisting structure for morphing applications". *Proc. R. Soc. A Math. Phys. Eng. Sci.,* ***468***(2141), pp. 1230–1251.

[24] Ratcliffe, J., Czabaj, M., and O'Brien, T., 2012. "Characterizing Delamination Migration in Carbon/Epoxy Tape Laminates". In 27th Am. Soc. Compos. Tech. Conf.

[25] Tsai, S., 1981. *Introduction to Composite Materials*. Technomic Publishing, Westport, CT.

[26] Girardeau-Montaut, D. CloudCompare Project. http://www.danielgm.net/cc/.

[27] Etches, J., Potter, K., Weaver, P., and Bond, I., 2009. "Environmental effects on thermally induced multistability in unsymmetric composite laminates". *Compos. Part A Appl. Sci. Manuf.,* ***40***(8), pp. 1240–1247.

[28] Telford, R., 2014. "Hygro-thermal Residual Stresses in Unsymmetrical Multi-Stable Composite Laminates". PhD thesis, University of Limerick.

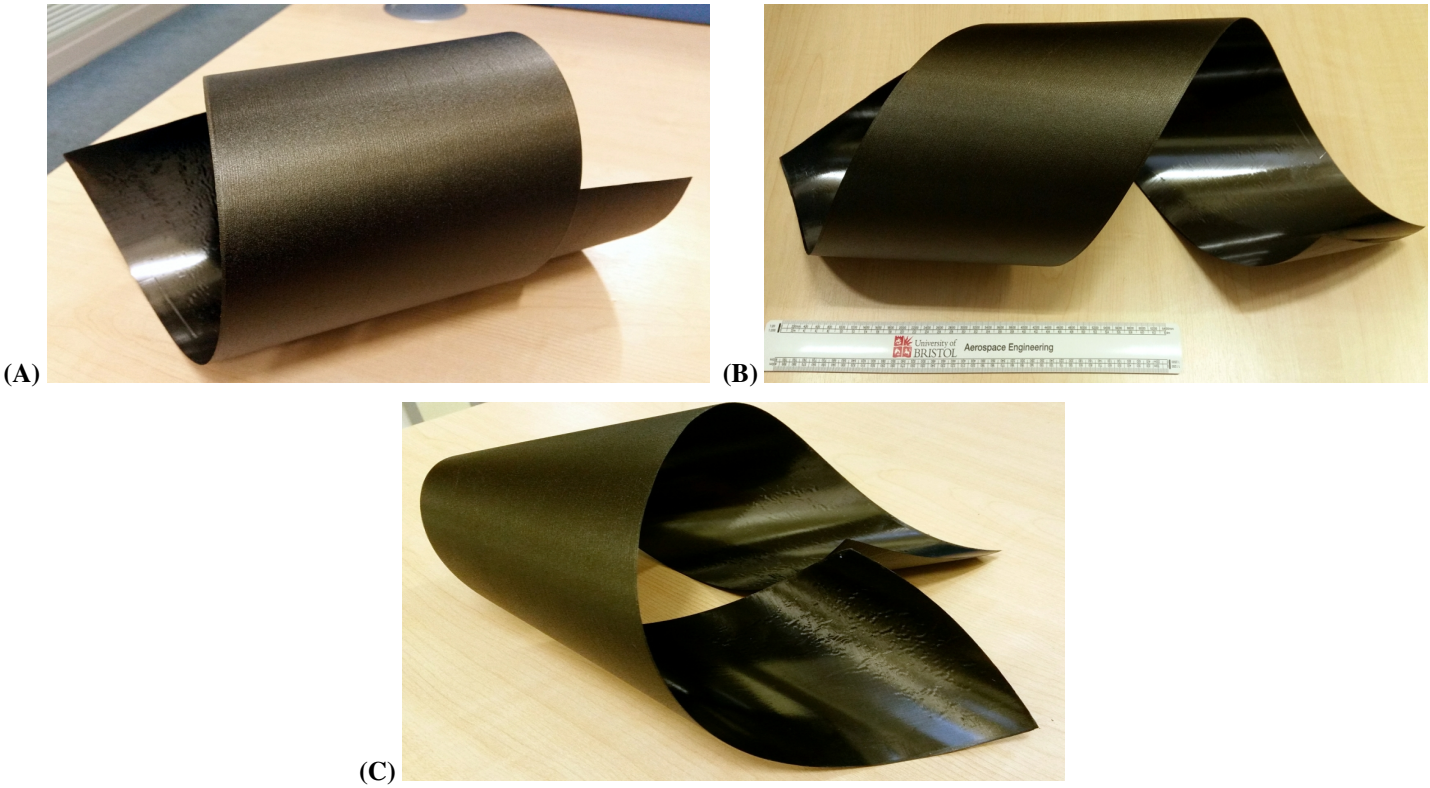

FIGURE 7. PHOTOS OF SAMPLE R50T1 SHOWING: (A) ITS ORIGINAL MONOSTABLE CONFIGURATION, (B) THE EXTENDED MONOSTABLE CONFIGURATION, AND (C) AN EXAMPLE OF A STABLE CONFIGURATION NOT PREDICTED BY ANY MODEL